ACES Asian Chemical Editorial Society

DOI: 10.1002/asia.201800729

CHEMISTRY AN ASIAN JOURNAL Full Paper

Supramolecular Chemistry

Multiprotein Dynamic Combinatorial Chemistry: A Strategy for the Simultaneous Discovery of Subfamily-Selective Inhibitors for Nucleic Acid Demethylases FTO and ALKBH3

Mohua Das, Tianming Yang, Jinghua Dong, Fransisca Prasetya, Yiming Xie, Kendra H. Q. Wong, Adeline Cheong, and Esther C. Y. Woon*[a]

Abstract: Dynamic combinatorial chemistry (DCC) is a powerful supramolecular approach for discovering ligands for biomolecules. To date, most, if not all, biologically templated DCC systems employ only a single biomolecule to direct the self-assembly process. To expand the scope of DCC, herein, a novel multiprotein DCC strategy has been developed that combines the discriminatory power of a zwitterionic "thermal tag" with the sensitivity of differential scanning fluorimetry. This strategy is highly sensitive and could differentiate the binding of ligands to structurally similar subfamily members. Through this strategy, it was possible to simultaneously identify subfamily-selective probes against two clinically important epigenetic enzymes: FTO (**7**; $IC_{50} = 2.6\ \mu M$) and ALKBH3 (**8**; $IC_{50} = 3.7\ \mu M$). To date, this is the first report of a subfamily-selective ALKBH3 inhibitor. The developed strategy could, in principle, be adapted to a broad range of proteins; thus it is of broad scientific interest.

Introduction

Dynamic combinatorial chemistry (DCC) is a powerful supramolecular approach for discovering ligands for biological targets. The idea was first independently conceived and developed by the Sanders and Lehn groups (for excellent reviews, see Refs [1–10]).[1–10] In the DCC method, simple building blocks are linked together by reversible covalent chemistry to generate dynamic libraries of structures. Because of the reversible nature of these libraries, they are highly responsive to external influence, such that the introduction of a template triggers the rapid structural adaptation of library members, which results in the assembly of structures that are highly complementary to the template. To date, DCC has been successfully applied to a range of biological templates, including enzymes, receptors, transmembrane transporters, nucleotides, and polymer-supported targets.[11–17] However, most, if not all, such biologically templated DCC approaches employ only a single template to direct the self-assembly process; this severely limits the applications of DCC approaches.

To expand the scope and potential of DCC, herein, we explored the concept of multiprotein DCC, through which two or more protein templates were used concurrently in the same dynamic system. We envisaged that such a strategy would enable the discovery of ligands against several proteins of interest simultaneously; thus greatly multiplying the power and efficiency of DCC. Another distinct advantage of the multiprotein DCC approach is that it permits the use of several structurally and/or functionally related protein isoforms in concert. This ensures that only ligands that are highly selective for a particular protein isoform or target will be assembled and identified. Although it is also possible to achieve highly selective inhibition from conventional DCC approaches (for instance, Greaney et al.[18] successfully identified isozyme-selective glutathione *S*-transferase inhibitors by using an acyl hydrazone based DCC), single-templated DCC systems only generate hits against one target at a time.

The development of the proposed multiprotein DCC system poses a number of analytical challenges. Not only is there a requirement to analyze several protein–ligand interactions simultaneously, it is also necessary to assign binding of ligands to specific proteins in a complex, multicomponent mixture. Furthermore, structures generated from reversible self-assembly systems are constantly exchanging, and this further complicates their analysis.

Currently, few methods have been reported for the analysis of single-templated DCC,[8,19] these include HPLC analysis;[20,21] NMR spectroscopy studies;[22–24] X-ray crystallography;[25] size-exclusion chromatography (SEC);[26,27] and, more recently, the use of polymer-scaffolded (PS-DCLs),[28] DNA,[29–32] or peptide nucleic acid (PNA)-encoded[33,34] dynamic combinatorial libraries (DCLs). However, these methods only detect amplification of the best binders in the presence of the template, and cannot distinguish which template is responsible for the ob-

[a] *M. Das, Dr. T. Yang, J. Dong, F. Prasetya, Y. Xie, K. H. Q. Wong, A. Cheong, Prof. E. C. Y. Woon*
Department of Pharmacy, National University of Singapore
18 Science Drive 4, Singapore 117543 (Singapore)
E-mail: esther.woon@nus.edu.sg

Supporting information and the ORCID identification number(s) for the author(s) of this article can be found under: https://doi.org/10.1002/asia.201800729.

served amplification; hence they are unsuitable for the proposed multiprotein DCC system. Although it is possible to directly observe different protein–ligand complexes through native protein MS techniques, the results of MS analyses are not always representative of what exists in solution because different noncovalent complexes survive the transition from solution to the gas phase differently.[35] Indeed, our group[14] and that of Poulsen[36] have previously observed fragmentation of protein–ligand complexes under certain MS ionization conditions. To date, no method exists that allow the analysis of multiple protein–ligand interactions in a dynamic system. This severely limits the potential applications of DCC-based approaches.

Recent studies have demonstrated that zwitterionic polymers, in general, are able to confer a wide range of biophysical properties if conjugated to proteins, such as increased water solubility, pH resistance, and antifouling properties.[37–40] More recently, Jiang et al. showed that poly(carboxybetaine) polymers and poly(Glu-Lys) polypeptides were able to improve the thermal stability of fusion partner proteins, rendering them more resistant to heat inactivation.[41,42]

Inspired by these interesting observations, herein, we present a novel detection strategy that enables the simultaneous analysis of several protein–ligand complexes in a multiprotein DCC system (Figure 1 A). It combines the discriminatory power of a thermal tag with the sensitivity of the differential scanning fluorimetry (DSF) technique. In this approach, the proteins of interest are genetically labeled with zwitterionic peptide-based thermal tags, which, by design, are capable of modifying the thermal stability of the host proteins without disrupting their structural and functional properties. The expectation is that, by appending appropriate thermal tags, one could specifically fine-tune the melting temperatures (T_m) of the proteins such that their individual melting profiles could be simultaneously monitored in a single DSF melting analysis. If used in combination with DCC, the formation of protein–ligand complexes can be easily detected by an increase in T_m of the proteins that are engaged in ligand binding.

This approach is conceptually similar to that of the DSF-based "thermal shift assay," which has been widely used for the detection of protein–ligand interactions with stable ligands.[43] However, prior to this work, it was not known whether DSF could be applied to the analysis of a DCL. We are also not aware of the combined use of a thermal tag with DSF to facilitate the study of multiple protein–ligand interactions. As we shall demonstrate, multiprotein DSF is a simple, yet powerful, strategy for monitoring protein-templated self-assembly. Through this method, one is able to assess T_m shifts and thermodynamic parameters of an equilibrating system in a single, rapid DSF experiment. We further provide proof of principle that the combined use of a multiprotein DSF strategy and DCC can enable the simultaneous templating of several target proteins. This is demonstrated by the concurrent discovery of subfamily-selective inhibitors against two clinically important epigenetic enzymes: FTO and ALKBH3.

To the best of our knowledge, the present study represents not only the first report of a multiprotein DCC method, but also a new strategy for probing dynamic chemical systems, which will hopefully further our understanding of protein-directed self-assembly, and inspire new applications for DCC-based approaches.

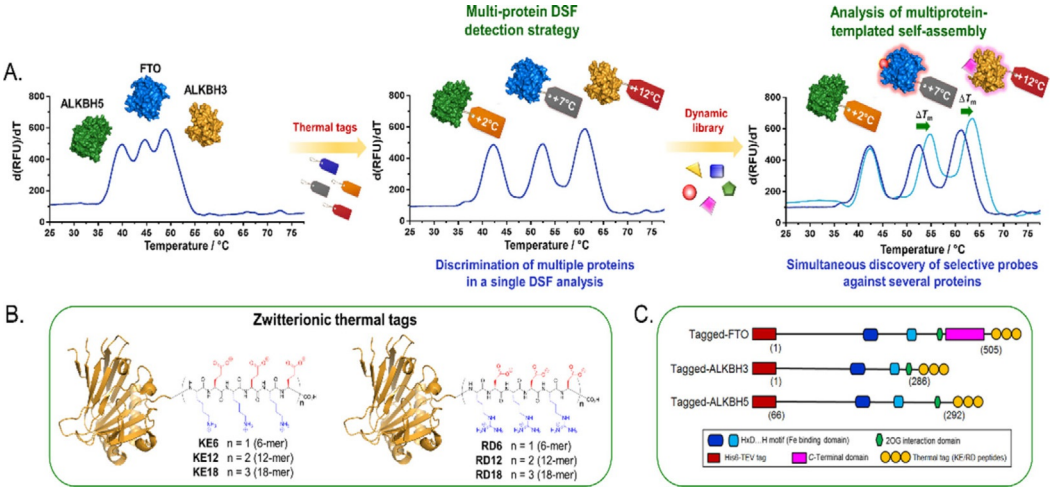

Figure 1. The multiprotein differential scanning fluorimetry (DSF) detection strategy and its application to a dynamic self-assembly system. A) In this approach, "thermal tags," which, by design, are capable of exclusively modulating the melting temperature of fusion partner proteins without compromising their structures and functions are used to fine-tune the melting temperature of the target proteins, such that their individual melting profiles could be simultaneously monitored in a single DSF melting analysis. If used in combination with DCC, the formation of stable protein–ligand complexes can be easily detected by shifts in T_m of proteins engaged in ligand binding. B) Structures of the thermal tags investigated herein. Both the KE and RD tags are zwitterionic peptides with alternating positively (blue) and negatively (red) charged amino acids. C) Schematic diagram of the fusion constructs. The KE and RD tags were genetically appended to the C terminus of FTO, ALKBH3, and ALKBH5; these are clinically important proteins belonging to the iron- and 2-oxoglutarate (2OG)-dependent AlkB oxygenases. The starting and terminating residue numbers of the proteins are given in parentheses. The fusion constructs also contain an N-terminal His_6-TEV TEV = tobacco etch virus) tag to facilitate protein purification (for details of expression and purification of the fusion proteins, see Supporting Information).

Results and Discussion

Thermal Tag Design and Protein Engineering

We selected three members of the iron- and 2OG-dependent AlkB oxygenases, namely, FTO, ALKBH3 and ALKBH5, as our protein templates.[44] These AlkB proteins are currently of intense biological and medical interest because of their critical roles in several key cellular processes, such as epigenetic gene regulation and RNA metabolism.[45–47] It is also increasingly clear that dysregulation of these enzymes may underlie the pathogenesis of a range of human diseases, including metabolic diseases, neurodegenerative diseases, and cancers.[48–51] However, despite their clinical significance, to date, there have been few reports of inhibitors that selectively target these enzymes, in part, owing to their close structural similarity, which renders the development of subfamily-selective inhibitors particularly challenging. In this regard, the selection of AlkB subfamilies for the present study not only allows us to evaluate the power of a multiprotein DCC strategy to simultaneously discover probes against several clinically important targets, but also its potential in directing the self-assembly of probes with subfamily selectivity.

To implement the proposed strategy (Figure 1 A), we first designed a series of thermal tags capable of conferring different melting temperatures to the AlkB proteins. As potential candidates, we considered short zwitterionic peptides that were 6, 12, or 18 residues in length, with either alternating Lys/Glu (KE) sequences (abbreviated as KE6-, KE12-, and KE18-tags) or alternating Arg/Asp (RD) sequences (abbreviated as RD6-, RD12-, and RD18-tags; Figure 1 B). Recent studies suggested that zwitterionic polymers, such as poly(carboxybetaine) polymers and poly(Glu-Lys) polypeptides, could increase the thermal resistance of fusion partner proteins.[41,42] However, we are not aware of the use of zwitterionic peptides to specifically modulate the melting temperature of proteins. The effect of zwitterionic peptides on the melting behavior of proteins has also not been systematically studied.

To investigate the suitability of zwitterionic peptides as thermal tags, the KE and RD sequences were genetically appended to the C termini of FTO, ALKBH3, and ALKBH5 through protein engineering techniques; modeling analysis suggests that fusion of a relatively short peptide to the C terminus of AlkB subfamilies is likely to be minimally disruptive on the structure and function of the protein (Figure 1 C; for details of gene constructs and protein expression, see the Supporting Information). Successful expression of all recombinant fusion proteins was confirmed by sodium dodecyl sulfate polyacrylamide gel electrophoresis (SDS-PAGE) and ESI-MS analyses (Figure S1 in the Supporting Information).

Introduction of a Single Thermal Tag to Trigger a Dramatic Increase in the Thermal Stability and Melting Temperature of the AlkB Subfamilies

We initially investigated the impact of thermal tags on protein melting characteristics. DSF-based melting analyses showed that all KE- and RD-tagged ALKBH5 fusion proteins unfolded cooperatively to produce monophasic melting transitions similar to that observed with unmodified ALKBH5; this implied that the proteins remained stably folded upon conjugation with KE or RD tags (Figure 2 A and Figure S2 A in the Supporting Information). The melting temperatures of the ALKBH5 fusion proteins are, however, significantly higher than that of unmodified ALKBH5 ($T_m = (40.3 \pm 0.1)\,^{\circ}C$; Table 1), which suggests a marked improvement in their thermal stability. The extent of thermal stabilization appears to be dependent on the length of the thermal tag used, as demonstrated by the observation that the relatively short KE6 tag increases the T_m of ALKBH5 by 2.1 °C, whereas longer KE12 and KE18 tags trigger more dramatic T_m increases of 4.9 and 9.2 °C, respectively. A similar trend (i.e., longer tag, leading to larger T_m increase) was also observed with RD tags, although correspondingly smaller T_m increases of 1.8, 3.4, and 8.2 °C were produced by RD6, RD12, and RD18 tags, respectively. Thus, the RD tags are slightly less effective at improving protein thermal stability than that of KE tags of the same length.

Table 1. Thermal stability data for ALKBH5, FTO, and ALKBH3, and their corresponding KE- and RD-tagged fusion proteins.[a]

Thermal tag	ALKBH5		FTO		ALKBH3	
	T_m [°C]	ΔT_m [°C]	T_m [°C]	ΔT_m [°C]	T_m [°C]	ΔT_m [°C]
untagged	40.3 ± 0.1	–	45.1 ± 0.2	–	49.4 ± 0.3	–
KE6	42.4 ± 0.2	2.1	48.3 ± 0.1	3.2	53.6 ± 0.1	4.2
KE12	45.2 ± 0.2	4.9	52.6 ± 0.2	7.5	57.4 ± 0.1	8.0
KE18	49.5 ± 0.3	9.2	55.4 ± 0.3	10.3	61.7 ± 0.1	12.3
RD6	42.1 ± 0.2	1.8	47.8 ± 0.1	2.7	52.5 ± 0.3	3.1
RD12	43.7 ± 0.1	3.4	49.7 ± 0.1	4.6	53.2 ± 0.1	3.8
RD18	48.5 ± 0.2	8.2	53.3 ± 0.2	8.2	57.9 ± 0.2	8.5

[a] The T_m values of the fusion proteins were measured at a protein concentration of 2 μM (in 50 mM HEPES buffer, pH 6.0) by means of DSF melting analysis.

Interestingly, the thermal stabilization effect of KE and RD tags also extends to other AlkB subfamilies, such as FTO and ALKBH3, for which modification of both proteins with either KE or RD tags again triggers a remarkable increase in T_m (Figure 2 and Figure S2 in the Supporting Information). As observed for ALKBH5, FTO, and ALKBH3, longer tags exhibit a larger T_m increase compared with that of their counterparts with shorter tags (Table 1). However, a KE tag of the same length appears to have a greater impact on ALKBH3 than those on FTO and ALKBH5. For instance, the KE18 tag produced a T_m increase of 12.3 °C in ALKBH3, but only 10.3 °C in FTO, and 9.2 °C in ALKBH5 (Table 1). In contrast, an RD tag of the same length triggered a similar T_m increase in all three proteins.

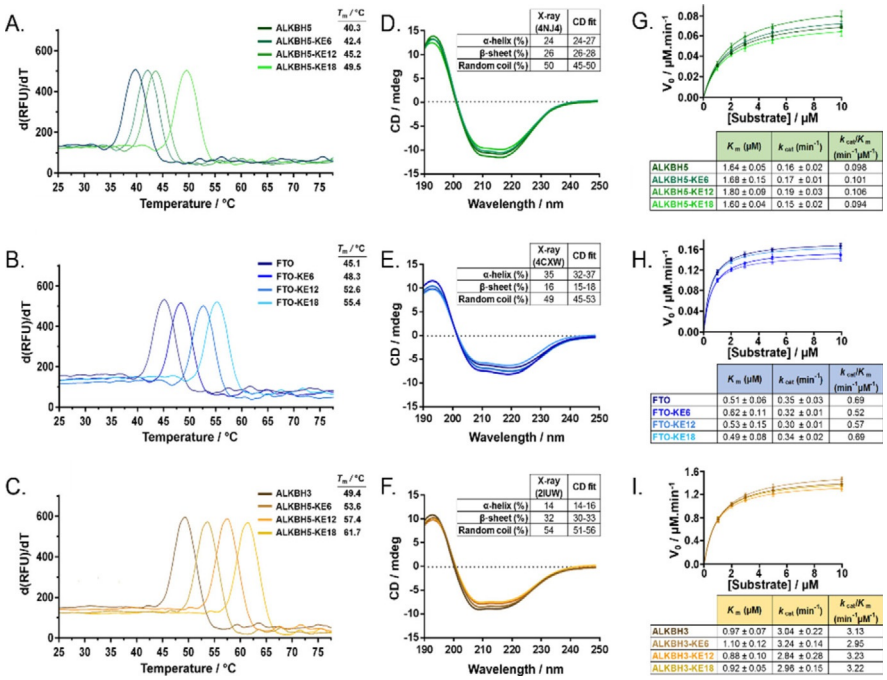

Figure 2. Effects of KE thermal tags on the thermal stability, structural conformation, and catalytic activity of AlkB demethylases (for the effects of RD thermal tags, see Figure S2 in the Supporting Information). Representative first-derivative plots showing the melting profiles of A) ALKBH5, B) FTO, and C) ALKBH3, and their corresponding KE-tagged fusion proteins (color-coded) at a protein concentration of 2 μM. In all cases, the introduction of a single KE tag triggered a significant increase in the melting temperature of the proteins. The extent of thermal stabilization increases with the length of the thermal tag used. D)–F) Superimposition of representative far-UV circular dichroism (CD) spectra for KE-tagged proteins and native proteins reveals negligible conformational changes in the presence of the KE tags. The insets show the secondary structure contents of the fusion proteins derived from fitting of the CD spectra; these are highly consistent with that of native proteins (obtained from X-ray crystal structures), suggesting that the fusion proteins remained natively folded upon conjugation with KE tags. G)–I) Steady-state kinetic analyses indicate that modification with the KE tag does not significantly alter the binding affinities and demethylase activities of AlkB enzymes. The K_m and k_{cat} values were determined by keeping a constant enzyme concentration of 0.5 μM. Error bars represent the standard deviation (SD) of three replicates.

These findings are notable because they suggest that the attachment of a single KE or RD tag as short as six residues in length is sufficient to induce a considerable change in the thermal stability and melting temperature of the fusion protein. It further suggests that one can, in principle, fine-tune the melting temperature of AlkB subfamilies by incorporating KE or RD tags of appropriate length. The mechanism by which the KE/RD tags enhance the melting temperatures of their partner proteins is unclear at present; nevertheless, it has been suggested that a zwitterionic peptide, which is strongly hydrophilic in nature, has the propensity to pull water away from the hydrophobic regions of the protein.[41,42] Presumably, this stabilizes the folded structure of the protein, and thus, increases its thermal stability and melting temperature. Alternatively, it could also result from ionic interactions between the protein and zwitterionic tag or a change in the oligomerization state of the fusion protein. Further studies are needed to understand the underlying mechanisms.

Impact of Thermal Tags on the Overall Conformation of the AlkB Subfamilies

Intriguingly, despite having a profound impact on thermal stability, the thermal tags do not significantly alter the overall secondary structures of the AlkB subfamilies, as clearly demonstrated by far-UV CD spectroscopy. In particular, all KE- and RD-tagged ALKBH5 proteins share well-ordered secondary structure elements, with a positive maximum at $\lambda \approx 194$ nm and a negative band at $\lambda \approx 215$ nm, which are similar to that observed for unmodified ALKBH5 (Figure 2D and Figure S2D in the Supporting Information). Spectral fitting further indicates approximately equal α-helical (≈24–27%) and β-sheet contents (≈26–28%) in all ALKBH5 fusion proteins, in agreement with the reported X-ray crystal structure of native ALKBH5 (PDB ID: 4NJ4).[52] Similarly, the CD characteristics and secondary structure contents of FTO and ALKBH3 fusion proteins are also highly consistent with that of their unmodified equivalents; this suggests that all thermally tagged proteins continue to adopt natively folded conformations (Figure 2E and F and Figure S2 in the Supporting Information; PDB ID: 4CXW[53] and 2IUW[54]).

Effect of Thermal Tags on the Catalytic Activity of the AlkB Subfamilies

We were also able to demonstrate that the thermal tags had little impact on the catalytic activities of AlkB demethylases. Notably, ALKBH5 and FTO preferentially demethylate N^6-methyladenosine (m^6A) substrates, whereas ALKBH3 favors N^1-methyladenosine (m^1A) substrates.[55,56] Consistent with their inher-

ent substrate specificity, detailed kinetic analyses revealed that ALKBH5 and FTO modified with either KE or RD tags displayed similar affinities (K_m) and catalytic efficiencies (k_{cat}/K_m) for the m^6A substrate as that of their unmodified proteins (Figure 2G and H and Figure S2 in the Supporting Information), whereas ALKBH3 conjugated with either KE or RD tags retained >90% of its canonical demethylase activity against the m^1A substrate (Figure 2I and Figure S2I in the Supporting Information). This finding is interesting because, contrary to our results, a previous study showed that the attachment of larger zwitterionic peptides, such as poly(Glu-Lys) 10 and 30 KDa in length, led to a significant increase in the substrate affinities of β-lactamases.[42] Apparently, a greater number of charged residues in longer peptides confers stronger hydrophilic properties that promote hydrophobic interactions between the substrate and its binding site. Our results therefore suggest that the effects of zwitterionic tags on protein activity could be reduced through the use of relatively short 6–18-mer peptide sequences. Moreover, the apparent lack of influence on protein conformations and catalytic activities further suggests that both KE and RD tags are likely to exist as separate entities that are structurally and functionally independent from the proteins to which they are attached.

Taken together, our results clearly demonstrate that both KE and RD tags are highly versatile thermal tags that are able to exclusively fine-tune the thermal stability and melting temperature of AlkB proteins, without compromising their structural conformation and catalytic activity. To the best of our knowledge, this is the first report to demonstrate that zwitterionic peptides could provide a general strategy for bioengineering proteins with the desired melting characteristics.

Recognition and Analysis of Multiple Proteins in a Mixture by Thermal Tags

To establish whether thermal-tag-induced T_m changes could facilitate the discrimination of different fusion proteins in the same mixture, we performed one-pot DSF analysis of a mixture of ALKBH5-KE6 (T_m = 42.4 °C), FTO-KE12 (T_m = 52.6 °C), and ALKBH3-KE18 (T_m = 61.7 °C); these proteins were selected because they had reasonably large differences in T_m. We appreciate that most proteins undergo aggregation during thermal unfolding; therefore, we were concerned that protein aggregates derived from the melting of one protein might interfere with the melting behavior of other proteins within the same mixture. Nevertheless, in our multiprotein DSF analysis, three distinct denaturation peaks were observed that resembled the melting profile of ALKBH5-KE6 superimposed with those of FTO-KE12 and ALKBH3-KE18; this suggests that mixing of fusion proteins does not significantly alter the individual melting characteristics (Figure 3A and B). Consistent with our detection strategy, there was also a marked separation of individual melting peaks (ΔT_m > 9 °C), which enabled any ligand-induced T_m shift to be clearly detected without merging of peaks, as demonstrated by ligand binding experiments with **1** (a known generic inhibitor of AlkB subfamilies)[57] and FTO-selective inhibitor **2** (PubChem ID: 126970771; Figure 3C and D).[53] By comparison, DSF analysis of a mixture of untagged ALKBH5, FTO, and ALKBH3 produced an overlapping melting profile that was difficult to deconvolute (Figure 3E). Thus, the combined use of thermal tags with DSF enables the simultaneous analysis of different fusion proteins in a mixture, even structurally similar subfamily members, which is otherwise challenging to differentiate.

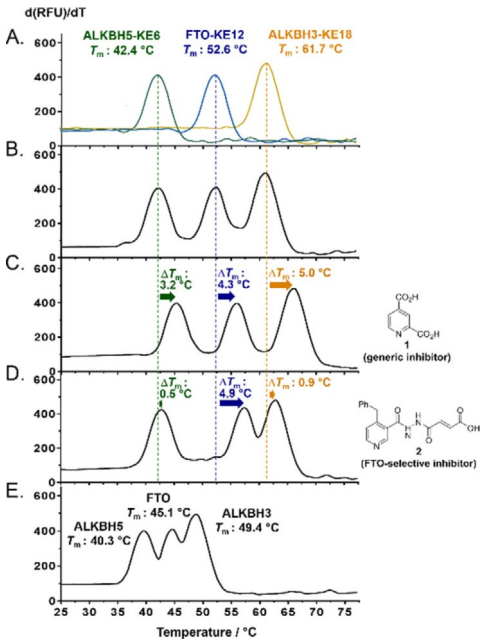

Figure 3. The thermal tags provide a basis for differential analysis of several proteins simultaneously. The DSF-based melting profiles of ALKBH5-KE6, FTO-KE12, and ALKBH3-KE18, upon being analyzed A) individually and B) as a mixture, revealed that the mixing of fusion proteins did not affect their individual melting behavior. Ligand binding experiments with C) generic inhibitor 2,4-pyridine dicarboxylic acid (**1**; 100 μM)[57] and D) FTO-selective inhibitor **2** (100 μM)[53] demonstrated the capability of the DSF detection strategy to monitor several protein–ligand interactions in a single DSF screen. E) DSF analysis of a mixture of unmodified ALKBH5, FTO, and ALKBH3 produced an overlapping melting profile to demonstrate the power of the thermal tag approach in discriminating structurally similar subfamily members.

Notably, in our multiprotein DSF strategy, different thermal tags were applied to different AlkB subfamilies. Hence, one possible issue is that fusion proteins with longer, more stabilizing tags might be less sensitive to further stabilization by ligands than those with shorter tags. However, the titration of each fusion protein against increasing concentrations of **1** revealed that proteins with the KE18 tag exhibited a similar concentration-dependent increase in T_m as those with KE12 and KE6 tags (Figure S3 in the Supporting Information). Thus, the length of the thermal tag used does not significantly impact on the magnitude of the ligand-induced T_m shift.

Analysis of Self-Assembly Dynamics by a Multiprotein DSF Detection Strategy

On the basis of these promising results, we next investigated whether the developed detection strategy could be used in combination with DCC to achieve multiprotein targeting. As our model dynamic reaction, we chose the reversible acyl hy-

drazone reaction between scaffold ligand **3** and aldehydes (Figure 4A). Acyl hydrazone exchange is one of the most well-established reversible reactions, first introduced by the Sanders group[58] and subsequently by others,[18,59,60] for the preparation of DCL. By design, scaffold **3** contains a hydrazide moiety that is free to participate in acyl hydrazone exchange with a set of aldehydes. It also contains a pyridyl function that, based on modeling analysis, is expected to bind to the AlkB subfamilies through chelation with the active site iron(II). Another notable feature is that **3** exhibits similar binding affinities for ALKBH5-KE6 ($K_{D,app}=(37.9\pm4)$ μM; $\Delta T_m=1.5$ °C), FTO-KE12 ($K_{D,app}=(40.4\pm4)$ μM; $\Delta T_m=0.7$ °C) and ALKBH3-KE18 ($K_{D,app}=(31.0\pm3)$ μM; $\Delta T_m=1.4$ °C); thus it does not inherently favor any particular protein template (Figures S6–S8 in the Supporting Information). The weak potency of **3** against all three proteins also enables the effect of hydrazone substitution to be monitored.

In a typical multiprotein DCC system, the DCL was set up by mixing all three fusion proteins, that is, ALKBH5-KE6 (2 μM), FTO-KE12 (2 μM), and ALKBH3-KE18 (2 μM), with $MnCl_2$ (50 μM; substitute for Fe^{II}) and scaffold **3** (40 μM), in the presence of 10 aldehydes, **4a–j**, each aldehyde at a concentration of 20 μM (library A; Figure 4B). The use of a fairly low concentration of aldehydes (10-fold relative to the individual protein concentration) was a deliberate strategy to detect only a high-affinity ligand. To facilitate rapid acyl hydrazone exchange, the reaction was performed under slightly acidic conditions (pH 6.0) in the presence of aniline (5 mM), which served as a nucleophilic catalyst.[18,61] Dynamic exchange was monitored by means of both DSF and HPLC analyses (Figure 5 and Figure S4 in the Supporting Information).

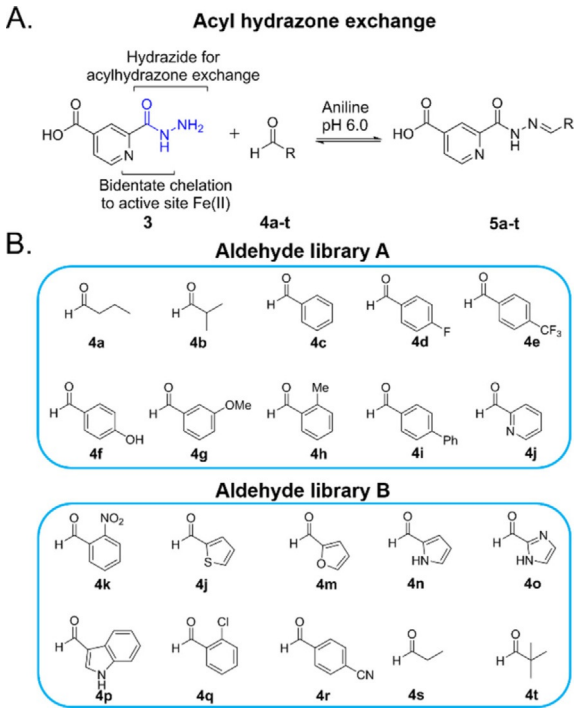

Figure 4. Formation of an acyl hydrazone DCL. A) Scaffold ligand **3** contains a pyridyl function that is expected to bind to the AlkB subfamilies through chelation with the active site Fe^{II}, which leaves the hydrazide side chain (blue) free to participate in acyl hydrazone exchange with aldehydes. To facilitate rapid acyl hydrazone exchange, the reaction was performed under slightly acidic conditions (pH 6.0) in the presence of a nucleophilic catalyst aniline.[48] B) Structures of aldehydes used in this study.

Initially, at t_0, the reaction mixture consisted predominantly of scaffold **3** and free aldehydes, with no apparent hydrazone adduct formation or T_m shift (Figure 5A and E). After 1 h of incubation, a distinct T_m shift could be detected for FTO-KE12 ($\Delta T_m=3.9$ °C; Figure 5B). This was likely to be induced by specific binding of **5e** to FTO-KE12, as supported by the concomitant amplification of hydrazone adduct **5e** in HPLC analysis (Figure 5F). As the reaction progressed, amplification of a second hydrazone adduct, **5h**, became apparent at 2 h, which resulted in a slight T_m shift for ALKBH3-KE18 ($\Delta T_m=2.7$ °C; Figure 5C and G). The T_m values of FTO-KE12 and ALKBH3-KE18 increased steadily over time, giving T_m shifts of 6.1 and 4.0 °C, respectively, after 5 h of incubation (Figure 5D and H). This was accompanied by an increase in amplification of **5e** and **5h** to about 35 and 32%, respectively, of total adduct concentration (Figure 5I). Detailed analysis revealed an excellent linear relationship between T_m shift and adduct concentration; hence, the magnitude of T_m shift provides a direct indication of the extent of adduct amplification (Figure 5J). Although some degree of fluorescence quenching occurred in the presence of the library components, the observed T_m shifts were highly reproducible (SD < 1 °C). To determine if heating of the DCL during DSF analysis could affect DCL equilibration, we performed HPLC analysis of the DCL at various temperatures, ranging from 37 to 70 °C (Figure S5 in the Supporting Information). The results revealed no significant change in DCL equilibration, even upon heating to 70 °C, although increasing DCL temperature did cause a decrease in retention time, which led to the merging of some adduct peaks.

The identity of the preferentially binding hydrazones was subsequently confirmed by separate DSF experiments, in which aldehydes **4a–j** were individually mixed with **3**, and then analyzed for T_m shift with the fusion proteins. This established adducts **5e** and **5h** as specific binders for FTO-KE12 and ALKBH3-KE18, respectively. Consistent with DCC results, no T_m shifts were observed for ALKBH5-KE6 for any combinations of **3** and aldehydes.

Multiprotein Targeting Enabled by Combined Use of Multiprotein DSF Detection with DCC

We appreciate that, to date, DSF analysis has primarily been used to study the binding of stable ligands to protein. Therefore, T_m shift data derived from labile and interchanging protein–ligand complexes may not reflect actual ligand binding affinity. To verify our multiprotein DCC results, we determined the binding affinities of the identified hits **5e** and **5h** by using NMR spectroscopy based water relaxation assays.[14,62] In this method, the apparent binding constants ($K_{D,app}$) were determined by monitoring the bulk water relaxation rate, which decreased if the access of water to paramagnetic manganese(II) in the active site was hindered through binding of ligands to the metal.

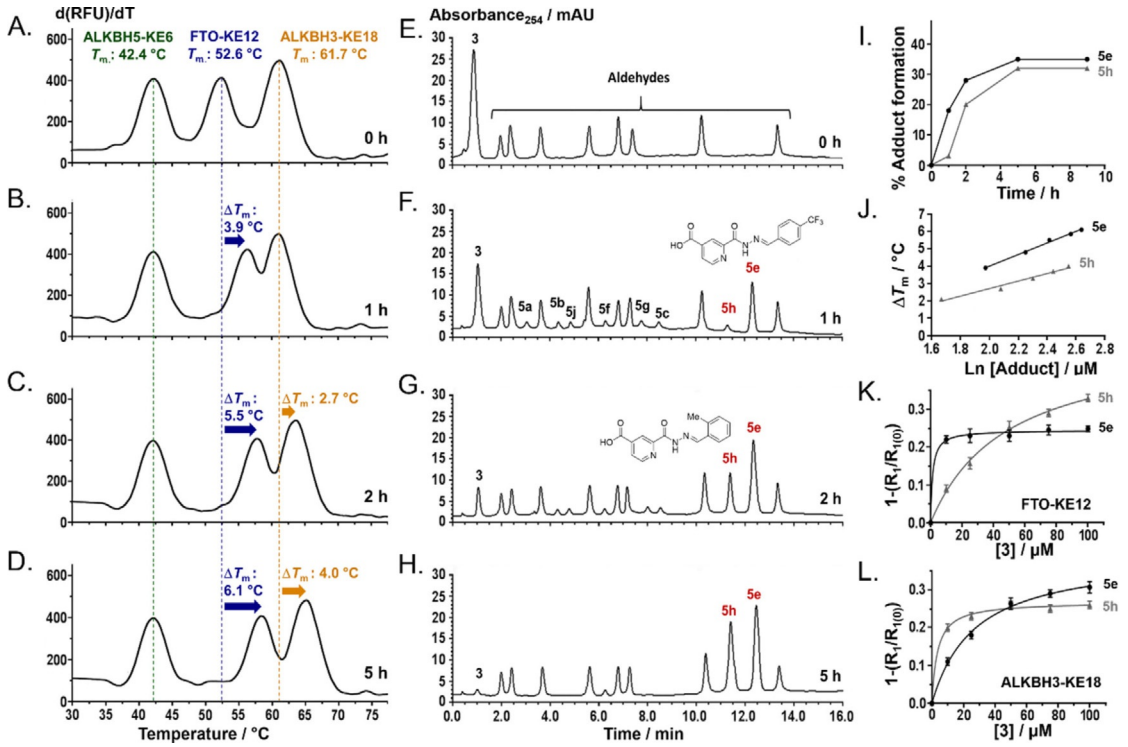

Figure 5. The multiprotein DSF detection strategy enables the analysis of self-assembly dynamics. The DCL was constituted by mixing ALKBH5-KE6 (2 µM), FTO-KE12 (2 µM), ALKBH3-KE18 (2 µM), scaffold ligand **3** (40 µM), aldehydes **4a–j** (library A, each aldehyde at 20 µM), $MnCl_2$ (50 µM), and aniline (5 mM) in HEPES buffer (50 mM, pH 6.0). A)–D) DSF melting analyses showed a time-dependent increase in T_m shift for FTO-KE12 and ALKBH3-KE18, which suggested the simultaneous assembly of hydrazone adducts capable of substantial binding to FTO-KE12 and ALKBH3-KE18. E)–H) HPLC analyses of the DCL revealed concomitant amplification of adducts **5e** and **5h**, at the expense of other hydrazone adducts. The peaks were assigned based on the retention times of pure aldehydes and adducts. I) The concentrations of the adducts were determined based on their respective HPLC peak areas, from calibration plots obtained with pure adducts. The percentages of adduct formation were calculated relative to the starting concentration of scaffold ligand **3** (40 µM). J) There is an excellent linear relationship between T_m shift and ln (adduct concentration); thus the magnitude of the T_m shift provides a direct indication of the extent of adduct amplification. NMR spectroscopy based water relaxation assay to confirm adducts **5e** and **5h** as specific binders for FTO-KE12 (K) and ALKBH3-KE18 (L). Error bars represent SD of three replicates.

Our NMR spectroscopy assays support results from DCC, in which a substantial increase in the binding affinity of **3** for FTO-KE12 ($K_{D,app}$ = (40.4 ± 4) µM) was observed only in the presence of aldehyde **4e** ($K_{D,app}$ (**5e**) = (0.46 ± 0.1) µM; Figure 5K); the presence of other aldehydes has a negligible effect on the binding affinity of **3** (Figure S6 in the Supporting Information). As anticipated, the affinity of **3** for ALKBH3-KE18 ($K_{D,app}$ = (31.0 ± 3) µM) was improved only in combination with aldehyde **4h** ($K_{D,app}$ (**5h**) = (1.0 ± 0.2) µM; Figure 5L), and not with other aldehydes (Figure S7 in the Supporting Information). Finally, the binding of **3** to ALKBH5-KE6 ($K_{D,app}$ = (37.9 ± 4) µM) was also not significantly altered by any of the aldehydes investigated (Figure S8 in the Supporting Information). Thus, there is a qualitative agreement between T_m shift data derived from DCC screening and ligand binding affinities. Our results therefore clearly demonstrated that the DSF technique could indeed be used to monitor and analyze self-assembly dynamics in multicomponent DCC systems.

Importantly, the successful identification of adducts **5e** and **5h** validates the capability of our multiprotein DCC approach to identify highly selective ligands against several targets simultaneously. Notably, adducts **5e** differ from **5h** by only a single isosteric replacement of *para*-CF_3 with an *ortho*-Me group; thus, this approach has the sensitivity to detect subtle active-site selectivity between structurally related subfamily members.

Comparing the Effects of Single and Multitemplating on Ligand Selection

We next compared the impact of single and multitemplating on ligand selection. We performed another set of DCC experiments, in which the DCL was constituted by mixing scaffold **3** and aldehydes **4k–t** (library B, Figure 4B). If the DCL was screened against each protein individually (single templating), we observed substantial binding of adduct **5k** to ALKBH5-KE6 (ΔT_m = 4.8 °C), FTO-KE12 (ΔT_m = 3.0 °C), and ALKBH3-KE18 (ΔT_m = 3.4 °C; Figure S9A–C in the Supporting Information). However, if the same DCL was screened against all three proteins concurrently (mulitemplating), the binding of **5k** to each protein was reduced to near-zero (ΔT_m values 0.1–0.3 °C; Figure S9D in the Supporting Information). DSF-based titration experiments further revealed that, if all three proteins were present, a considerably higher concentration of **5k** (≈31 µM) was required to produce a significant T_m shift of 1.0 °C in FTO-KE12, compared with only about 3 µM if only FTO-KE12 was present

(Figure S10 in the Supporting Information). In sharp contrast, the binding of selective ligands to their protein targets was not affected by the presence or absence of other proteins. For instance, the binding of **5e** (10 μM) to FTO-KE12 elicits a similar T_m shift of about 5 °C whether in the presence of a single or multiple protein templates (Figure S9E,F in the Supporting Information). Importantly, in a DCL containing both selective and nonselective adducts **5e** and **5k** (set up by adding aldehyde **4e** (20 μM) to the above DCL), only the specific binding of **5e** to FTO-KE12 could be detected (Figure S9G in the Supporting Information). Taken together, the results suggest that the extent of T_m shifts in multitemplating DCC experiments is primarily dependent on the affinity of the ligands for the target proteins. Presumably, strong binders, such as **5e**, dominate the DCL equilibrium at the expense of weak binders, such as **5k**, whereas weak binders dominate the DCL equilibrium over nonbinders.

Identification of Subfamily-Selective Probes for FTO and ALKBH3 by Multiprotein DCC

To establish whether the hits identified from our multiprotein DCC screening were active inhibitors of AlkB demethylases, we synthesized stable analogues of **5c**, **5e**, **5h**, and **5k**, wherein the relatively labile acyl hydrazone moiety was replaced with a stable sulfonamide moiety (Scheme 1). It should be emphasized that the key result of any DCC experiment is information about the most effective structural combinations of the building blocks. Hence, labile groups, such as hydrazones, are often replaced to form stable ligands.[63]

The resulting stable analogues, **6**–**9**, were evaluated for activity against a panel of untagged AlkB subfamilies by using both HPLC-based demethylase assays and T_m shift assays (for assay conditions, see the Supporting Information).

As shown in Figure 6, the T_m shift and inhibition data are in close agreement with the multiprotein DCC results. In particu-

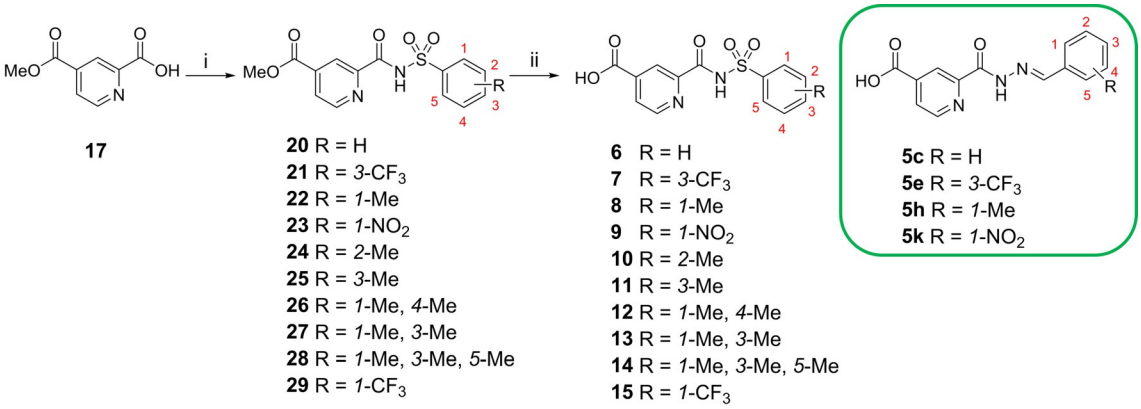

Scheme 1. Synthesis of stable sulfonamide analogues **6**–**15**. Compounds **6**–**9** are stable analogues of identified hydrazone hits **5c**, **5e**, **5h**, and **5k**, respectively, wherein the relatively labile acyl hydrazone moiety is replaced by a stable sulfonamide moiety. Reagents and conditions: i) substituted benzenesulfonamides, Et_3N, 1-hydroxybenzotriazole hydrate, 1-ethyl-3-(3-dimethylaminopropyl)carbodiimide hydrochloride, CH_2Cl_2, 25 °C; ii) LiOH, tetrahydrofuran–water (4:1), 25 °C. See the Experimental Section and Supporting Information for full synthesis, characterization, and NMR spectra of compounds.

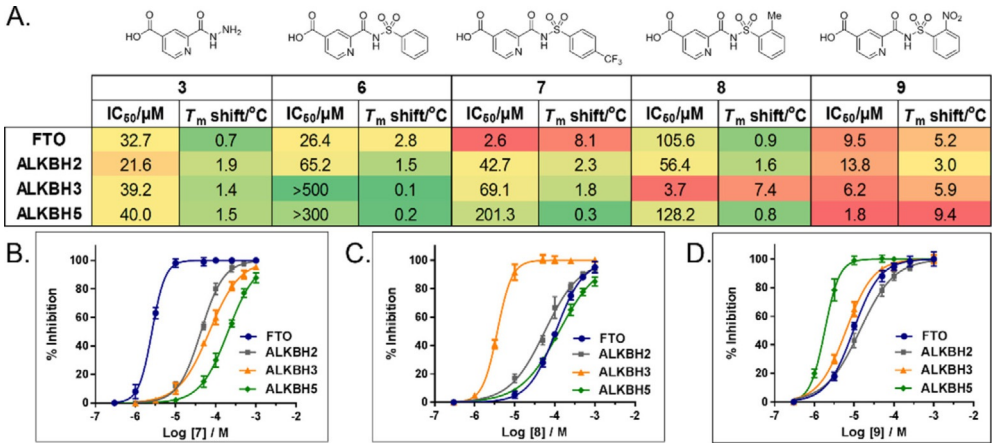

Figure 6. Activity profiling of the sulfonamide analogues against representative AlkB subfamilies. A) Consistent with multiprotein DCC results, compound **7** demonstrates distinct selectivity for FTO, with substantially reduced inhibition and T_m shift against other AlkB subfamilies, whereas **8** exhibits >100-fold selectivity for ALKBH3 over FTO and ALKBH5. Compounds **7** and **8** also discriminate against other human 2OG oxygenases, as demonstrated by their poor inhibitory activities against JMJD2A (IC_{50} >100 μM). The reported values are an average of three replicates. Enzyme inhibition curves of B) **7**, C) **8**, and D) **9**, as determined from the HPLC-based assay. Error bars represent SD of three replicates. For enzyme inhibition curves of compounds **3** and **6**, see Figure S11 in the Supporting Information.

lar, compounds **7** (analogue of **5e**) and **8** (analogue of **5h**) were indeed potent inhibitors of FTO ($IC_{50}=2.6\ \mu M$, $\Delta T_m=8.1\,^{\circ}C$) and ALKBH3 ($IC_{50}=3.7\ \mu M$, $\Delta T_m=7.4\,^{\circ}C$), respectively, with IC_{50} values in the low micromolar range, which represents more than 10-fold improvement in activity compared with that of scaffold ligand **3**. Notably, compound **9** (analogue of **5k**), which was identified by the single-templated DCC, was also found to be a relatively potent, nonselective inhibitor, and control compound **6** (analogue of **5c**) a poor inhibitor against all AlkB enzymes investigated ($IC_{50}>25\ \mu M$).

The selectivity profiles of compounds **7** and **8** are also strikingly consistent with the multiprotein DCC results (Figure 6). In particular, we observed remarkable selectivity of **7** for FTO, with substantially reduced inhibition and T_m shifts against ALKBH3 ($IC_{50}=69.1\ \mu M$, $\Delta T_m=1.8\,^{\circ}C$) and ALKBH5 ($IC_{50}=201.3\ \mu M$, $\Delta T_m=0.3\,^{\circ}C$), whereas **8** exhibited >100-fold greater activity for ALKBH3 over those of FTO ($IC_{50}=105.6\ \mu M$, $\Delta T_m=0.9\,^{\circ}C$) and ALKBH5 ($IC_{50}=128.2\ \mu M$, $\Delta T_m=0.8\,^{\circ}C$). Further profiling studies revealed that **7** and **8** also discriminated against other human 2OG oxygenases, as demonstrated by their poor inhibitory activities against ALKBH2 (IC_{50}s >40 μM) and JMJD2A (IC_{50}s >100 μM; a histone demethylase critically involved in chromatin remodeling).[64] Our results therefore validate the multiprotein DCC screening as a reliable method for the simultaneous identification of subfamily-selective probes.

To rationalize the selectivity of **7** and **8**, a series of mono-, di-, and trimethyl-substituted analogues, **10**–**15**, were prepared and evaluated for activities against the AlkB subfamilies. The assay results are summarized in Figure 7 and suggest that the introduction of a methyl substituent at the *ortho* position (i.e., **8**) favors ALKBH3 selectivity, whereas shifting it to either the *meta* (i.e., **10**) or *para* positions (i.e., **11**) drives the selectivity towards FTO. This change in selectivity was particularly apparent upon comparing the activity of **8** with that of analogues **12**–**14**. In all cases, the addition of either a *meta*- or *para*-methyl groups caused a substantial increase in selectivity towards FTO.

A similar trend was also observed for **7**, whereby a translocation of the trifluoromethyl substituent from the *para* to *ortho* positions (i.e., **15**) resulted in a 14-fold reduction in potency against FTO, coupled with an increase (3-fold) in potency towards ALKBH3 (Figure 7B). Notably, these substitutions have very little or no effect on the activities towards ALKBH2 and ALKBH5. Structural models of complexes of FTO–**7** and ALKBH3–**7**, which were built by using the reported crystal structures of FTO (PDB ID 4CXW[53]) and ALKBH3 (PDB ID 2IUW;[54] Figure 8), reveal that compound **7** is able to coordinate with the active site iron(II) in a bidentate manner and participate in hydrogen-bonding interactions with the side chains of Arg96 (2.4 and 2.5 Å). The pyridyl carboxylate group is further stabilized through the formation of salt bridges with both N^{ω} of Arg319 (2.5 and 2.7 Å), and hydrogen bonds with the hydroxyl groups of Tyr295 (2.7 Å) and Ser318 (2.6 Å). Modeling studies further suggest that **7** might not be able to fit into the binding pocket of ALKBH3, owing to potential steric clash between the 4-trifluoromethylphenyl group and the side chain of Tyr143. This may contribute to the poor activity of **7** against ALKBH3 (Figure 8B). However, the proposed model is unable to account for the activity of compounds **8** and **15** because similar steric clash is also possible between these compounds and ALKBH3. Further crystallographic studies are needed to determine the exact structural basis for the selectivity of these inhibitors. Studies are also currently underway to determine the potency and selectivity of **7** and **8** in cells, which will provide insights into their usefulness as functional probes and, possibly, therapeutic leads.

A.

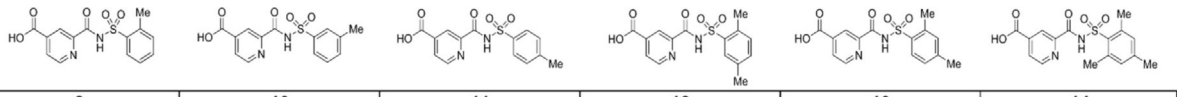

	8		10		11		12		13		14	
	IC_{50}/μM	T_m shift/°C	IC_{50}/μM	T_m shift/°C	IC_{50}/μM	T_m shift/°C	IC_{50}/μM	T_m shift/°C	IC_{50}/μM	T_m shift/°C	IC_{50}/μM	T_m shift/°C
FTO	105.6	0.9	5.8	5.2	4.6	6.7	4.0	6.9	7.9	4.6	5.2	6.3
ALKBH2	56.4	1.6	56.6	1.7	25.8	2.5	10.8	3.3	85.3	1.1	106.9	0.7
ALKBH3	3.7	7.4	11.4	3.0	23.3	2.8	25.1	2.7	41.3	2.5	21.2	2.5
ALKBH5	128.2	0.8	>300	0.3	75.5	1.3	>300	0.2	68.4	1.5	>300	0.3

B.

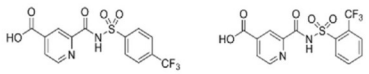

	7		15	
	IC_{50}/μM	T_m shift/°C	IC_{50}/μM	T_m shift/°C
FTO	2.6	8.1	36.7	2.0
ALKBH2	42.7	2.3	46.2	1.8
ALKBH3	69.1	1.8	22.5	2.9
ALKBH5	201.3	0.3	>300	0.1

Figure 7. Selectivity studies of analogues of A) ALKBH3-selective inhibitor **8**, and B) FTO-selective inhibitor **7**. In all compounds investigated, the introduction of a methyl or trifluoromethyl substituent at the *ortho* position favors ALKBH3 selectivity, whereas a translocation of these groups to the *meta* or *para* positions promotes FTO selectivity; this is apparent from a comparison of the selectivity profile of **8** with those of **10** and **11**, or that of **7** with **15**. Likewise, the addition of either *meta*- or *para*-methyl groups to **8** (i.e., **12**–**14**) drives the selectivity towards FTO. The reported values are an average of three replicates.

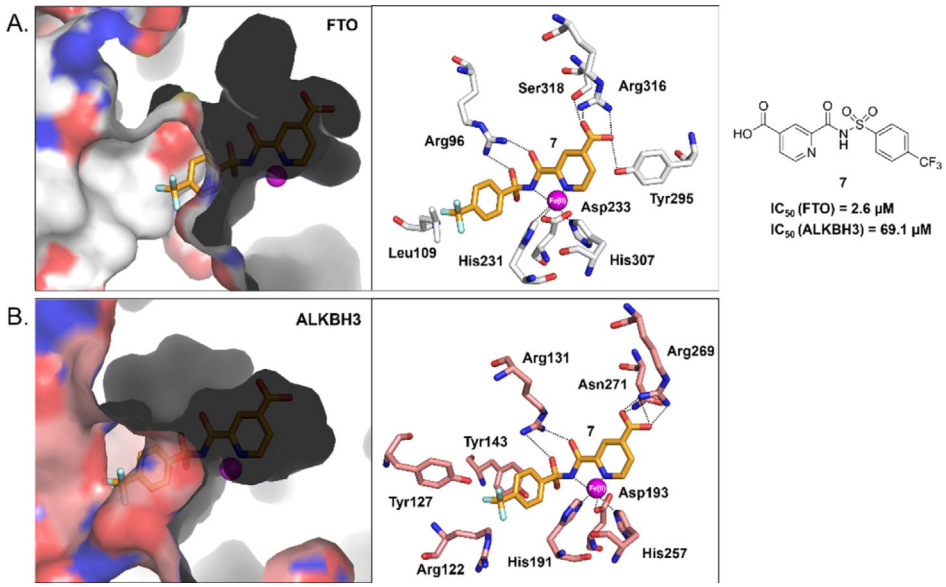

Figure 8. Rationalization of the selectivity of **7** for FTO over ALKBH3. The structural models of the A) FTO–**7** complex, and B) ALKBH3–**7** complex are built by using the reported crystal structures of FTO (white surface and white sticks; PDB ID 4CXW[53]) and ALKBH3 (salmon surface and salmon sticks; PDB ID 2IUW[54]). The right panels show close-up views of interactions between **7** and active-site residues in FTO and ALKBH3. Whereas **7** forms highly favorable interactions with FTO, it is unable to fit into the binding pocket of ALKBH3, owing to steric clash between the 4-trifluoromethylphenyl group and the side chain of Tyr143.

Conclusion

Overall, we used a combination of protein engineering, spectroscopic, thermodynamic, kinetic, biochemical, and thermal denaturation studies to investigate the effects of zwitterionic tags on protein structures and functions. Our results revealed that the incorporation of a single KE or RD peptide, as short as 6 to 18 residues in length, could trigger a dramatic increase in thermal stability and melting temperature of the host proteins without disrupting their structural conformations and catalytic activities. We further showed that both KE and RD tags were highly versatile thermal tags and generally applicable to a range of proteins, including AlkB subfamilies, such as FTO, ALKBH3, and ALKBH5. To the best of our knowledge, this is the first report to show that zwitterionic peptides can be used to exclusively fine-tune the melting temperature of proteins. Importantly, by exploiting thermal-tag-induced T_m changes, we developed a novel DSF-based detection strategy that enabled analysis of several protein–ligand interactions simultaneously. The assay is remarkably sensitive and could effectively distinguish the binding of ligands to different proteins, including structurally similar subfamily members, which is extremely challenging to achieve. Through the combined use of multiprotein DSF and DCC, we were able to achieve simultaneous discovery of highly selective probes against several target proteins. This was demonstrated by the identification of compounds **7** and **8**, which not only exhibited exceptional selectivity for FTO ($IC_{50}=2.6\ \mu M$, $\Delta T_m=8.1\ ^\circ C$) and ALKBH3 ($IC_{50}=3.7\ \mu M$, $\Delta T_m=7.4\ ^\circ C$), respectively, over other AlkB subfamilies, but also discriminated against structurally related human 2OG oxygenases, such as JMJD2A. Notably, to date, there are no reports of subfamily-selective ALKBH3 inhibitors. In light of the biological and clinical significance of FTO and ALKBH3, we envisaged that the identified inhibitors would be of interest as functional probes and, possibly, therapeutic leads.

One limitation of this approach is that it is only applicable to proteins that are amenable to T_m modification by thermal tags. Conceivably, the use of a larger number of proteins will produce significant T_m signal overlap, and this limits the number of protein templates that can be analyzed concurrently. Moreover, it is necessary to carry out separate experiments to determine the identity of the best binders. Nevertheless, the method is relatively simple, cheap, and amenable to a high-throughput format. Moreover, unlike current techniques, such as HPLC and NMR spectroscopy analyses, it detects ligand binding, rather than amplification of the best binders, which greatly simplifies spectral analysis; thus potentially permitting the use of larger, more complex DCLs. Although this study focuses on the development of multiprotein DCC, the developed method is highly versatile and may, in principle, be adapted to a wide range of studies, such as the parallel profiling of compound libraries, high-throughput mapping of protein substrate specificity, and the study of protein–protein/nucleic acid interactions. Thus, the approach outlined herein is of general scientific interest.

To the best of our knowledge, this study represents not only the first example of multiprotein DCC, but also a new strategy for probing dynamic chemical systems, which will hopefully further our understanding of protein-directed self-assembly, and inspire new applications for DCC-based approaches.

Experimental Section

General

Starting materials, reagents, and solvents were obtained from commercial sources and used as received. Progress of the reactions was monitored by TLC, which was performed on precoated aluminum-backed plates (Merck, silica 60 F254). Purification of intermediates and final products was carried out by using flash column chromatography conducted on silica gel (230–400 mesh). Melting points were determined by using a Gallenkamp melting point apparatus. IR spectra were recorded on a PerkinElmer Spectrum 100 FTIR spectrometer by using neat compound. ^{1}H and ^{13}C NMR spectra were recorded by using tetramethylsilane (TMS) as an internal standard with a Bruker Advance 400 Ultrashield NMR spectrometer at 400 and 100 MHz, respectively. Chemical shifts (δ) were reported in ppm downfield from TMS. The signals were quoted as s (singlet), d (doublet), t (triplet), m (multiplet), and br (broad). Coupling constants, *J*, were given in Hz (±0.5 Hz). ESI-MS spectra were recorded on a Shimadzu LC-MS2020 mass spectrometer. HRMS was recorded by using a Bruker MicroTOF-QII mass spectrometer. The purity of synthesized compounds was confirmed to be higher than 95% by means of analytical reverse-phase HPLC (Ultimate 3000). Compound **1** was commercially available and used without any further purification. Compound **2** was synthesized as previously reported.[53] The synthesis and characterization of selected compounds, **7**, **8**, **17**, **21**, and **22**, are described below. For the synthesis of other compounds investigated herein, see the Supporting Information.

Synthesis of 17

An aqueous solution of sodium hydroxide (1.2 mL, 6 M) was added to a solution of dimethyl pyridine-2,4-dicarboxylate (**16**; 1.4 g, 7.3 mmol) in methanol (20 mL). The mixture was then stirred at room temperature for 10 h, after which time the solvent was evaporated in vacuo. The resulting residue was washed with ethyl acetate (20 mL), dissolved in water (40 mL) and the aqueous solution was acidified to pH 2 with concentrated HCl at 0 °C. The mixture was then filtered to give **17** (368 mg, 28%) as a white solid. M.p. 230–231 °C; ^{1}H NMR (400 MHz, [D$_6$]DMSO): δ = 3.92 (s, 3H; CO_2CH_3), 8.05 (d, J = 3.6 Hz, 1H), 8.38 (s, 1H), 8.91 (d, J = 4.4 Hz, 1H), 13.95 ppm (s, 1H; CO_2H); ^{13}C NMR (100 MHz, [D$_6$]DMSO): δ = 52.5 (CO_2CH_3), 123.4, 126.0, 139.4, 148.4, 150.9, 164.5 (CO_2CH_3), 165.2 ppm (CO_2H); IR (neat): $\tilde{\nu}$ = 1707 cm^{-1} (CO); MS (ESI$^-$): *m/z*: 180.3 [*M*−H]$^-$.

Synthesis of 21

Triethylamine (301 mg, 2.9 mmol), 1-hydroxybenzotriazole hydrate (172 mg, 1.2 mmol), and 1-(3-dimethylaminopropyl)-3-ethylcarbodiimide hydrochloride (245 mg, 1.2 mmol) were added sequentially at room temperature to a suspension of 4-(methoxycarbonyl)picolinic acid (**17**; 154 mg, 0.8 mmol) in dichloromethane (3 mL). The reaction was stirred at room temperature for 30 min before 4-(trifluoromethyl)benzenesulfonamide (230 mg, 1 mmol) was added. The reaction mixture was stirred at room temperature for 3 days. The reaction mixture was then diluted with dichloromethane and washed with an aqueous solution of citric acid (10%). The organic layer was neutralized by an aqueous saturated solution of $NaHCO_3$ and dried over anhydrous Na_2SO_4. Then the solvent was removed in vacuo and the residue was purified by flash column chromatography (dichloromethane/methanol 10:1). The fractions collected were further purified by triturating with *n*-hexane/isopropanol and the precipitate was separated by filtration to give **21** as a white solid (268 mg, 81%). R_f = 0.60 (dichloromethane/methanol 4:1); m.p. 230–231 °C; IR (neat): $\tilde{\nu}$ = 1170 (SO), 1263 (CF), 1353, 1730 cm^{-1} (CO); ^{1}H NMR (400 MHz, [D$_6$]DMSO): δ = 3.89 (s, 3H; CO_2CH_3), 7.79 (m, 2H), 7.86 (m, 2H), 8.02 (m, 1H), 8.44 (s, 1H), 8.71 ppm (m, 1H); ^{13}C NMR (100 MHz, [D$_6$]DMSO): δ = 52.3 (CO_2CH_3), 123.4, 123.9 (q, ^{1}J(C,F) = 270.8 Hz), 124.8 (q, ^{3}J(C,F) = 3.7 Hz), 125.5, 127.8, 133.1 (q, ^{2}J(C,F) = 31.7 Hz), 147.3, 147.5, 149.4, 150.0, 165.1 (CONH), 167.0 ppm (CO_2CH_3); ^{19}F NMR (376.3 MHz, [D$_6$]DMSO): δ = 61.20 ppm; MS (ESI$^-$): *m/z*: 387.1 [*M*−H]$^-$.

Synthesis of 7

Lithium hydroxide monohydrate (15.3 mg, 0.3 mmol) was added to a solution of methyl 2-({[4-(trifluoromethyl)phenyl]sulfonyl}carbamoyl)isonicotinate (**21**; 59.5 mg, 0.1 mmol) in tetrahydrofuran/water (1:1, 4 mL). The reaction mixture was stirred at room temperature for 18 h. The aqueous layer was washed with dichloromethane and then acidified to pH 1 by using an aqueous solution of hydrochloric acid (2 N). The precipitate was separated by filtration to give **7** (40.5 mg, 70%) as a white solid. M.p. 252–253 °C; IR (neat): $\tilde{\nu}$ = 1274 (CF), 1167 (SO), 1362, 1657 (CO), 1716 (CO), 3007 cm^{-1} (OH); ^{1}H NMR (400 MHz, [D$_6$]DMSO): δ = 8.01 (m, 3H), 8.20 (m, 2H), 8.42 (s, 1H), 8.85 ppm (m, 1H); ^{13}C NMR (100 MHz, [D$_6$]DMSO): δ = 122.0, 123.4 (q, ^{1}J(C,F) = 271.3 Hz), 125.1, 126.3 (q, ^{3}J(C,F) = 3.7 Hz), 127.4, 128.7, 133.0 (q, ^{2}J(C,F) = 32.2 Hz), 140.9, 143.6, 149.0, 150.2, 164.3 (CONH), 165.3 ppm (CO_2H); ^{19}F NMR (376.3 MHz, [D$_6$]DMSO): δ = 61.65 ppm; MS (ESI$^-$): *m/z*: 373.1 [*M*−H]$^-$; HRMS (ESI): *m/z* calcd for $C_{14}H_8F_3N_2O_5S$ [*M*−H]$^-$: 373.0112; found: 373.0115.

Synthesis of 22

Triethylamine (549 mg, 5.4 mmol), 1-hydroxybenzotriazole hydrate (314 mg, 2.3 mmol), and 1-(3-dimethylaminopropyl)-3-ethylcarbodiimide hydrochloride (441 mg, 2.3 mmol) were added sequentially at room temperature to a suspension of **17** (280 mg, 1.5 mmol) in dichloromethane (5 mL). The reaction mixture was stirred at room temperature for 30 min before *o*-toluenesulfonamide (292 mg, 1.7 mmol) was added. The reaction mixture was stirred at room temperature for 48 h, diluted with dichloromethane, and washed with an aqueous solution of citric acid (10%). The organic layer was neutralized with an aqueous saturated solution of $NaHCO_3$ and dried over anhydrous Na_2SO_4. Then the solvent was removed in vacuo and the residue was purified by flash column chromatography (dichloromethane/methanol 10:1). The fractions collected were further purified by triturating with *n*-hexane/isopropanol and the precipitate was separated by filtration to give **22** as a white solid (70.9 mg, 13%). R_f = 0.60 (dichloromethane/methanol 4:1); m.p. 265–266 °C; IR (neat): $\tilde{\nu}$ = 1175 (SO), 1349, 1709 cm^{-1} (CO); ^{1}H NMR (400 MHz, [D$_6$]DMSO): δ = 2.53 (s, 3H; CH_3), 3.89 (s, 3H; CO_2CH_3), 7.16–7.18 (m, 1H), 7.22–7.32 (m, 2H), 7.89–7.90 (m, 1H), 7.94 (dd, J = 4.8, 1.4 Hz, 1H), 8.45 (m, 1H), 8.87 ppm (d, J = 4.7 Hz, 1H); ^{13}C NMR (100 MHz, [D$_6$]DMSO): δ = 20.1 (CH_3), 52.3 (CO_2CH_3), 123.3, 124.8, 125.5, 128.4, 129.9, 130.9, 135.7, 143.9, 147.5, 147.9, 149.9, 165.2 (CONH), 166.5 ppm (CO_2CH_3); MS (ESI$^-$): *m/z*: 333.1 [*M*−H]$^-$.

Synthesis of 8

Lithium hydroxide monohydrate (12.2 mg, 0.2 mmol) was added to a solution of methyl 2-[(*o*-tolylsulfonyl)carbamoyl]isonicotinate (**22**; 49 mg, 0.1 mmol) in tetrahydrofuran/water (1:1, 8 mL). The reaction mixture was stirred at room temperature for 10 h. The aqueous layer was washed with dichloromethane and acidified to pH 1 with

an aqueous solution of hydrochloric acid (2 N). The precipitate was separated by filtration to give **8** as a white solid (23.7 mg, 51%). M.p. 246–247 °C; IR (neat): $\tilde{\nu}=1149$ (SO), 1342, 1638 (CO), 1651 (CO), 3006 cm^{-1}; ^1H NMR (400 MHz, [D_6]DMSO): $\delta=2.61$ (s, 3H; CH_3), 7.40–7.47 (m, 2H), 7.60 (m, 1H), 7.97 (m, 1H), 7.98 (m, 1H), 8.43 (m, 1H), 8.86 ppm (m, 1H); ^{13}C NMR (100 MHz, [D_6]DMSO): $\delta=$ 19.6 (CH_3), 122.6, 124.9, 126.2, 130.4, 132.4, 133.7, 137.1, 137.2, 140.1, 149.2, 150.5, 163.6 (CONH), 165.4 ppm (CO_2H); (OH); MS (ESI$^-$): *m/z*: 319.1 $[M-H]^-$; HRMS (ESI): *m/z* calcd for $C_{14}H_{11}N_2O_5S$ $[M-H]^-$: 319.0394; found: 319.0934.

Plasmid and Thermal Tag Construction

DNA fragments encoding full-length human FTO and N-terminally truncated ALKBH5 (residues 66–292) were cloned into pNIC28-Bsa4 to generate N-terminal His_6-tagged $FTO_{1\text{-}505}$ and N-terminal His_6-tagged $ALKBH5_{66\text{-}292}$ constructs, respectively, as previously described.[53,55] DNA for full-length human ALKBH3 was cloned into pET28a to generate an N-terminal His_6-tagged $ALKBH3_{1\text{-}286}$ construct, as previously described.[56] The above constructs were then subjected to mutagenesis experiments by using the QuikChange mutagenesis kit (Agilent Technologies), whereby DNA encoding various KE and RD tag sequences (commercially synthesized by GenScript USA) was fused to the C terminus of the respective genes. The sequences of all fusion protein constructs were confirmed by DNA sequencing.

Protein Expression and Purification

Full-length human FTO,[47,53,55] human ALKBH3,[56] human $ALKBH5_{66\text{-}292}$,[53,55] human $ALKBH2_{56\text{-}258}$,[46,53,56] and human $JMJD2A_{1\text{-}359}$[53] was expressed and purified as previously reported, with modifications. In brief, all constructs for the proteins and their KE/RD tagged fusion proteins were transformed into *Escherichia coli* BL21 (DE3) Rosetta cells. The transformed cells were grown at 37 °C until an optical density at $\lambda=600$ nm (OD600) of 0.6 was reached. Protein expression was then induced with isopropyl β-D-1-thiogalactopyranoside (IPTG; 0.5 mM, Gold Biotechnology). Cell growth was continued at 16 °C for 16 h, after which time cells were harvested by centrifugation and the resulting cell pellet was stored at −80 °C. The frozen cell pellets were then thawed, resuspended in lysis buffer, and disrupted by using a French Press. Further purification of the protein was achieved by using Ni affinity chromatography and gel filtration, as described below.

Full-length human FTO was subcloned into pNIC28-Bsa4 to generate a His_6-tagged $FTO_{1\text{-}505}$ construct. FTO in lysis buffer (25 mM Tris, pH 7.5, 500 mM NaCl, 40 mM imidazole, and 5 mM β-mercaptoethanol (β-ME) was purified through Ni affinity chromatography (GE healthcare), followed by gel filtration by using HiLoad Superdex 200 26/60 (GE healthcare) in the final buffer (25 mM Tris buffer, pH 7.5, 100 mM NaCl, 5% (v/v) glycerol and 5 mM β-ME).

Full-length ALKBH3 was subcloned into pET28a to generate a His_6-tagged $ALKBH3_{1\text{-}286}$ construct. ALKBH3 in lysis buffer (50 mM sodium phosphate, pH 8.0, 300 mM NaCl, 10 mM imidazole, and 5 mM β-ME) was purified through Ni affinity chromatography (GE healthcare), followed by gel filtration by using HiLoad Superdex 75 16/60 (GE healthcare) in the final buffer (25 mM sodium phosphate buffer, pH 8.0, 150 mM NaCl, 5% (v/v) glycerol, and 5 mM β-ME).

For human ALKBH5, a His_6-tagged $ALKBH5_{66\text{-}292}$ construct in pNIC28-Bsa4 was used. ALKBH5 in lysis buffer (20 mM Tris, pH 8.0, 500 mM NaCl, 40 mM imidazole, and 5 mM β-ME) was first purified through Ni affinity chromatography (GE healthcare), followed by anion chromatography with a 5 mL HiTrap Q HP column (GE healthcare) and gel filtration by using HiLoad Superdex 75 16/60 (GE healthcare) in the final buffer (20 mM Tris buffer, pH 8.0, 100 mM NaCl, and 5 mM β-ME).

For human ALKBH2, a His_6-tagged $ALKBH2_{56\text{-}258}$ construct in pET28b was used. ALKBH2 in lysis buffer (50 mM sodium phosphate buffer, pH 8.0, 300 mM NaCl, 10% (v/v) glycerol, 5 mM β-ME) was purified through Ni affinity chromatography (GE healthcare), followed by anion chromatography with a 5 mL HiTrap Q HP column (GE healthcare) and gel filtration by using HiLoad Superdex 75 26/60 (GE healthcare) in the final buffer (10 mM Tris, pH 8.0, 100 mM NaCl, and 5 mM β-ME).

For human JMJD2A, a His_6-tagged $JMJD2A_{1\text{-}359}$ construct in pNIC28-Bsa4 was used. The transformed *E. coli* cells were grown in Terrific Broth (TB) supplemented with 8 $g\,L^{-1}$ of glycerol and appropriate antibiotics. JMJD2A in lysis buffer containing 100 mM HEPES, 500 mM NaCl, 10 mM imidazole, 10% glycerol, 0.5 mM tris(2-carboxyethyl)phosphine (TCEP), pH 8.0, benzonase, and Protease Inhibitor Cocktail Set III was purified by using a Ni-NTA Superflow (Qiagen) column followed by a HiLoad 16/60 Superdex-200 column (GE Healthcare) in the final buffer (20 mM HEPES, pH 7.5, 300 mM NaCl, 10% (v/v) glycerol, 0.5 mM TCEP). All KE/RD-tagged proteins were expressed by using similar methods. For details, see the Supporting Information.

DSF Melting Analysis

All DSF-based experiments were performed by using a MiniOpticon real-time PCR detection system (Bio-Rad), monitoring protein unfolding by using SYPRO orange (Invitrogen), according to the reported method.[43,53]

Characterization of the Effects of Thermal Tags on the T_m of Proteins

The reaction mixtures contained proteins (2 μM), $MnCl_2$ (50 μM; active site metal), and 5× SYPRO orange (Invitrogen; fluorescent dye) in a final volume of 50 μL. Reagents were prepared in 50 mM HEPES buffer, pH 6.0, except $MnCl_2$, which was dissolved as 100 mM stock solutions in 20 mM HCl, then further diluted in MilliQ water. Fluorescence was detected on the FAM channel, with readings taken every 0.5 °C in the range of 25–95 °C; the temperature increased linearly by 1 °C min^{-1}. The fluorescence intensity data was then fitted to a Boltzmann sigmoidal curve by using the GraphPad Prism 6.0 program to determine the T_m values of the proteins. The T_m shift caused by the thermal tags was determined by the subtraction of T_m of untagged protein from T_m of the fusion protein. The assay was performed in triplicate for each protein, with SDs typically <1 °C.

Thermal Shift Assay with Inhibitors

The reaction mixtures contained proteins (2 μM), $MnCl_2$ (50 μM), compounds (100 μM), and 5× SYPRO in a final volume of 50 μL. The inhibitors tested were prepared in 100% dimethyl sulfoxide (DMSO) and added such that the final concentration of DMSO was not more than 1% v/v of assay mix. The T_m value was determined as described above. The T_m shift caused by the addition of each inhibitor was determined by subtraction of the reference T_m (derived from protein incubated with $MnCl_2$ and 1% v/v DMSO) from the T_m obtained in the presence of the inhibitor. The assay was performed in triplicate for each inhibitor, with SDs typically <1 °C.

CD Spectroscopy

The proteins were exchanged into 10 mM sodium phosphate buffer (pH 6.0). Far-UV CD spectra were recorded at a protein concentration of 0.1 mg mL^{-1} at 25 °C on a JASCO J-810 spectropolarimeter over a wavelength range of $\lambda = 190–250$ nm at a scan rate of 20 nm min^{-1}. All spectra were subtracted with the buffer blank and smoothed by using the Savitsky–Golay algorithm (polynomial order 10). All measurements were performed in triplicate.

Steady-State Kinetic Analyses of Nucleic Acid Demethylation by Untagged ALKB Proteins and Their Tagged Counterparts

Steady-state kinetic analysis was performed by using HPLC-based demethylation assays. The substrates used were 5′-GG(m^{6}A)CU-3′ (for FTO), 5′-AAAGCAG(m^{1}A)ATTCGAA-3′ (for ALKBH3), and 5′-GG(m^{6}A)CU-3′ (for ALKBH5). The K_m and k_{cat} values were determined by keeping a constant enzyme concentration of 0.5 μM and varying the substrate concentrations (0.5, 1, 2, 3, 5, and 10 μM), as previously reported.[53] The concentration of demethylated product at different substrate concentrations was plotted as a function of time. The initial velocity (V_0) for each substrate concentration was determined from the slope of the curve at the beginning of a reaction. The Michaelis–Menten curve was fitted by means of nonlinear regression, and the kinetic constants (V_{max}, K_m) of the substrate were estimated by using the GraphPad Prism 6.0 program. All reactions were performed at 4 °C in triplicate and adjusted to ensure that less than 20% of the substrate was consumed.

Multiprotein DCC Approach

The DCL was constituted by mixing ALKBH5-KE6 (2 μM), FTO-KE12 (2 μM), ALKBH3-KE18 (2 μM), scaffold ligand **3** (40 μM), aldehydes **4a–j** (library A, each aldehyde at 20 μM), $MnCl_2$ (50 μM), and aniline (5 mM) in HEPES buffer (50 mM, pH 6.0) in a final reaction volume of 50 μL. The reaction was incubated at 25 °C for the specified time points (Figure 5), after which time SYPRO orange (5×; Invitrogen) was added, and the reaction mixture analyzed by using a MiniOpticon™ real-time PCR detection system (Bio-Rad). Melting curves were obtained by steady heating from 25 to 95 °C at a rate of 1 °C min^{-1}. Fluorescence was detected on the FAM channel, with readings taken every 0.5 °C. The fluorescence intensity data was then fitted to a Boltzmann sigmoidal curve by using the GraphPad Prism 6.0 program to determine T_m of the proteins. The assay was performed in triplicate, with SDs typically < 1 °C.

HPLC Analysis of Multiprotein DCC

The DCL was analyzed by using a Zorbax C18 column (4.6 mm × 250 mm) at a flow rate of 1 mL min^{-1} at 25 °C. Gradient used: from 95% solvent A (water + 0.1% trifluoroacetic acid (TFA)) to 15% solvent B (MeOH) over 20 min, then to 60% solvent B over 30 min. The UV detection wavelength was set at $\lambda = 254$ nm. The concentration of adducts **5e** and **5h** was calculated based on their peak areas, from calibration plots obtained from pure standards. The percentages of adduct formation were calculated relative to the starting concentration of scaffold ligand **3** (40 μM).

NMR Spectroscopy Water Relaxation Experiments

The NMR spectroscopy assay was performed as previously reported, with modifications.[14,65] The experiments were conducted at 500 MHz by using a Bruker DRX 500 spectrometer equipped with a standard 5 mm *z*-gradient TXI probe. Unless otherwise stated, all experiments were conducted at 298 K in conventional 3 mm diameter NMR tubes (Norell). A freshly prepared mixture of protein (50 μM), Mn^{II} (50 μM), and aldehyde (500 μM) buffered with 50 mM Tris dissolved in 10% H_2O and 90% D_2O (pH 6.0) was titrated against scaffold ligand **3** at varying concentrations (10, 25, 50, 80, 100 μM). A 1:1 molar ratio of protein to Mn^{II} was used to minimize any contribution to relaxation rate changes from binding of small molecules to free Mn^{II}. Inversion recovery experiments were performed with two scans with a relaxation delay of at least $5 \times T_1$ (longitudinal relaxation time constants) between transients. Pulse tip-angle calibration by using the single-pulse nutation method was undertaken for each sample to ensure accurate 90 and 180° pulses. Data were plotted as the fractional change in relaxation rate ($1 - R_1/R_{1(0)}$) against ligand concentration. K_D curves were fitted by using the GraphPad Prism 6.0 program. The assay was performed in triplicate.

Acknowledgements

This research was supported by grants from the Singapore Ministry of Health's National Medical Research Council (NMRC/BNIG/2008/2013) and the Singapore Ministry of Education (AcRF Tier 1 Grant R148-000-231-114 and R148-000-238-114).

Conflict of interest

The authors declare no conflict of interest.

Keywords: drug discovery · dynamic combinatorial chemistry · epigenetics · inhibitors · proteins

[1] P. T. Corbett, J. Leclaire, L. Vial, K. R. West, J. L. Wietor, J. K. M. Sanders, S. Otto, *Chem. Rev.* **2006**, *106*, 3652–3711.
[2] J.-M. Lehn, *Chem. Soc. Rev.* **2007**, *36*, 151–160.
[3] O. Ramström, L. Amorim, R. Caraballo, O. Norberg in *Dynamic Combinatorial Chemistry* (Eds.: J. N. Reek, S. Otto), Wiley-VCH, Weinheim, **2010**, pp. 109–150.
[4] O. Ramström, J.-M. Lehn, *Nat. Rev. Drug Discovery* **2002**, *1*, 26–36.
[5] M. Mondal, A. K. H. Hirsch, *Chem. Soc. Rev.* **2015**, *44*, 2455–2488.
[6] C. Karan, B. L. Miller, *Drug Discovery Today* **2000**, *5*, 67–75.
[7] A. Herrmann, *Chem. Soc. Rev.* **2014**, *43*, 1899–1933.
[8] R. van der Vlag, A. K. H. Hirsch, *Analytical Methods in Protein-Templated Dynamic Combinatorial Chemistry in Comprehensive Supramolecular Chemistry II* (Ed.: J. L. Atwood), Elsevier, Amsterdam, **2017**, pp. 487–509.
[9] R. Huang, I. K. H. Leung, *Molecules* **2016**, *21*, 910.
[10] M. Jaegle, E. L. Wong, C. Tauber, E. Nawrotzky, C. Arkona, J. Rademann, *Angew. Chem. Int. Ed.* **2017**, *56*, 7358–7378; *Angew. Chem.* **2017**, *129*, 7464–7485.
[11] M. Mondal, N. Radeva, H. Köster, A. Park, C. Potamitis, M. Zervou, G. Klebe, A. K. H. Hirsch, *Angew. Chem. Int. Ed.* **2014**, *53*, 3259–3263; *Angew. Chem.* **2014**, *126*, 3324–3328.
[12] E. C. Y. Woon, M. Demetriades, E. A. L. Bagg, W. Aik, S. M. Krylova, J. H. Y. Ma, M. Chan, L. J. Walport, D. W. Wegman, K. N. Dack, M. A. McDonough, S. N. Krylov, C. J. Schofield, *J. Med. Chem.* **2012**, *55*, 2173–2184.
[13] N. R. Rose, E. C. Y. Woon, G. L. Kingham, O. N. F. King, J. Mecinović, I. J. Clifton, S. S. Ng, J. Talib-Hardy, U. Oppermann, M. A. McDonough, C. J. Schofield, *J. Med. Chem.* **2010**, *53*, 1810–1818.
[14] M. Demetriades, I. K. H. Leung, R. Chowdhury, M. C. Chan, M. A. McDonough, K. K. Yeoh, Y. M. Tian, T. D. W. Claridge, P. J. Ratcliffe, E. C. Y. Woon, C. J. Schofield, *Angew. Chem. Int. Ed.* **2012**, *51*, 6672–6675; *Angew. Chem.* **2012**, *124*, 6776–6779.
[15] B. L. Miller in *Constitutional Dynamic Chemistry in Topics in Current Chemistry* (Ed: M. Barboiu), Springer, Heidelberg, **2012**, pp. 107–137.
[16] C. S. Mahon, D. A. Fulton, *Nat. Chem.* **2014**, *6*, 665–672.

[17] B. P. Benke, P. Aich, Y. Kim, K. L. Kim, M. R. Rohman, S. Hong, I. C. Hwang, E. H. Lee, J. H. Roh, K. Kim, *J. Am. Chem. Soc.* **2017**, *139*, 7432 – 7435.
[18] V. T. Bhat, A. M. Caniard, T. Luksch, R. Brenk, D. J. Campopiano, M. F. Greaney, *Nat. Chem.* **2010**, *2*, 490 – 497.
[19] M. C. Misuraca, E. Moulin, Y. Ruff, N. Giuseppone, *New J. Chem.* **2014**, *38*, 3336 – 3349.
[20] S. Zameo, B. Vauzeilles, J. M. Beau, *Eur. J. Org. Chem.* **2006**, 5441 – 5444.
[21] L. Roy, M. A. Case, *J. Phys. Chem. B* **2011**, *115*, 2454 – 2464.
[22] M. Dal Molin, G. Gasparini, P. Scrimin, F. Rastrelli, L. J. Prins, *Chem. Commun.* **2011**, *47*, 12476.
[23] Y. Cohen, L. Avram, L. Frish, *Angew. Chem. Int. Ed.* **2005**, *44*, 520 – 554; *Angew. Chem.* **2005**, *117*, 524 – 560.
[24] K. K. Larson, M. He, J. F. Teichert, A. Naganawa, J. W. Bode, *Chem. Sci.* **2012**, *3*, 1825 – 1828.
[25] M. S. Congreve, D. J. Davis, L. Devine, C. Granata, M. O'Reilly, P. G. Wyatt, H. Jhoti, *Angew. Chem. Int. Ed.* **2003**, *42*, 4479 – 4482; *Angew. Chem.* **2003**, *115*, 4617 – 4620.
[26] J. F. Folmer-Andersen, J.-M. Lehn, *Angew. Chem. Int. Ed.* **2009**, *48*, 7664 – 7667; *Angew. Chem.* **2009**, *121*, 7800 – 7803.
[27] D. A. Fulton, *Org. Lett.* **2008**, *10*, 3291 – 3294.
[28] C. S. Mahon, M. A. Fascione, C. Sakonsinsiri, T. E. McAllister, W. Bruce Turnbull, D. A. Fulton, *Org. Biomol. Chem.* **2015**, *13*, 2756 – 2761.
[29] F. V. Reddavide, W. Lin, S. Lehnert, Y. Zhang, *Angew. Chem. Int. Ed.* **2015**, *54*, 7924 – 7928; *Angew. Chem.* **2015**, *127*, 8035 – 8039.
[30] J. P. Daguer, M. Ciobanu, S. Alvarez, S. Barluenga, N. Winssinger, *Chem. Sci.* **2011**, *2*, 625 – 632.
[31] Z. Kanlidere, O. Jochim, M. Cal, U. Diederichsen, *Beilstein J. Org. Chem.* **2016**, *12*, 2136 – 2144.
[32] G. Li, W. Zheng, Z. Chen, Y. Zhou, Y. Liu, J. Yang, Y. Huang, X. Li, *Chem. Sci.* **2015**, *6*, 7097 – 7104.
[33] M. Egholm, O. Buchardt, L. Christensen, C. Behrens, S. M. Freier, D. A. Driver, R. H. Berg, S. K. Kim, B. Norden, P. E. Nielsen, *Nature* **1993**, *365*, 566 – 568.
[34] H. D. Urbina, F. Debaene, B. Jost, C. Bole-Feysot, D. E. Mason, P. Kuzmic, J. L. Harris, N. Winssinger, *ChemBioChem* **2006**, *7*, 1790 – 1797.
[35] J. M. Daniel, S. D. Friess, S. Rajagopalan, S. Wendt, R. Zenobi, *Int. J. Mass Spectrom.* **2002**, *216*, 1 – 27.
[36] S.-A. Poulsen, *J. Am. Soc. Mass Spectrom.* **2006**, *17*, 1074 – 1080.
[37] S. Jiang, Z. Cao, *Adv. Mater.* **2010**, *22*, 920 – 932.
[38] L. Zheng, H. S. Sundaram, Z. Wei, C. Li, Z. Yuan, *React. Funct. Polym.* **2017**, *118*, 51 – 61.
[39] L. Mi, S. Jiang, *Angew. Chem. Int. Ed.* **2014**, *53*, 1746 – 1754; *Angew. Chem.* **2014**, *126*, 1774 – 1782.
[40] P. Zhang, F. Sun, C. Tsao, S. Liu, P. Jain, A. Sinclair, H.-C. Hung, T. Bai, K. Wu, S. Jiang, *Proc. Natl. Acad. Sci. USA* **2015**, *112*, 12046 – 12051.
[41] A. J. Keefe, S. Jiang, *Nat. Chem.* **2012**, *4*, 59 – 63.
[42] E. J. Liu, A. Sinclair, A. J. Keefe, B. L. Nannenga, B. L. Coyle, F. Baneyx, S. Jiang, *Biomacromolecules* **2015**, *16*, 3357 – 3361.
[43] F. H. Niesen, H. Berglund, M. Vedadi, *Nat. Protoc.* **2007**, *2*, 2212 – 2221.
[44] A. Thalhammer, W. Aik, E. A. L. Bagg, C. J. Schofield, *Drug Discovery Today Ther. Strategies* **2012**, *9*, e91 – e100.
[45] S. C. Trewick, T. F. Henshaw, R. P. Hausinger, T. Lindahl, B. Sedgwick, *Nature* **2002**, *419*, 174 – 178.
[46] C.-G. Yang, C. Yi, E. M. Duguid, C. T. Sullivan, X. Jian, P. A. Rice, C. He, *Nature* **2008**, *452*, 961 – 965.
[47] G. Jia, Y. Fu, X. Zhao, Q. Dai, G. Zheng, Y. Yang, C. Yi, T. Lindahl, T. Pan, Y.-G. Yang, C. He, *Nat. Chem. Biol.* **2011**, *7*, 885 – 887.
[48] G. Zheng, J. A. Dahl, Y. Niu, P. Fedorcsak, C. M. Huang, C. J. Li, C. B. Vågbø, Y. Shi, W. L. Wang, S. H. Song, Z. Lu, R. P. Bosmans, Q. Dai, Y. J. Hao, X. Yang, W. M. Zhao, W. M. Tong, X. J. Wang, F. Bogdan, K. Furu, Y. Fu, G. Jia, X. Zhao, J. Liu, H. E. Krokan, A. Klungland, Y. G. Yang, C. He, *Mol. Cell* **2013**, *49*, 18 – 29.
[49] T. M. Frayling, N. J. Timpson, M. N. Weedon, E. Zeggini, R. M. Freathy, C. M. Lindgren, J. R. B. Perry, K. S. Elliott, H. Lango, N. W. Rayner, B. Shields, L. W. Harries, J. C. Barrett, S. Ellard, C. J. Groves, B. Knight, A. M. Patch, A. R. Ness, S. Ebrahim, D. A. Lawlor, S. M. Ring, Y. Ben-Shlomo, M. R. Jarvelin, U. Sovio, A. J. Bennett, D. Melzer, L. Ferrucci, R. J. Loos, I. Barroso, N. J. Wareham, F. Karpe, K. R. Owen, L. R. Cardon, M. Walker, G. A. Hitman, C. N. Palmer, A. S. Doney, A. D. Morris, G. D. Smith, A. T. Hattersley, M. I. McCarthy, *Science* **2007**, *316*, 889 – 894.
[50] K. Koike, Y. Ueda, H. Hase, K. Kitae, Y. Fusamae, S. Masai, T. Inagaki, Y. Saigo, S. Hirasawa, K. Nakajima, I. Ohshio, Y. Makino, N. Konishi, H. Yamamoto, K. Tsujikawa, *Curr. Cancer Drug Targets* **2012**, *12*, 847 – 856.
[51] A. Lim, J. Zhou, R. A. Sinha, B. K. Singh, S. Ghosh, K. H. Lim, P. K. H. Chow, E. C. Woon, P. M. Yen, *Biochem. Biophys. Res. Commun.* **2016**, *479*, 476 – 481.
[52] W. Aik, J. S. Scotti, H. Choi, L. Gong, M. Demetriades, C. J. Schofield, M. A. McDonough, *Nucleic Acids Res.* **2014**, *42*, 4741 – 4754.
[53] J. D. W. Toh, L. Sun, L. Z. M. Lau, J. Tan, J. J. A. Low, C. W. Q. Tang, E. J. Y. Cheong, M. J. H. Tan, Y. Chen, W. Hong, Y.-G. Gao, E. C. Y. Woon, *Chem. Sci.* **2015**, *6*, 112 – 122.
[54] O. Sundheim, C. B. Vågbø, M. Bjørås, M. M. L. Sousa, V. Talstad, P. A. Aas, F. Drabløs, H. E. Krokan, J. A. Tainer, G. Slupphaug, *EMBO J.* **2006**, *25*, 3389 – 3397.
[55] S. Zou, J. D. W. Toh, K. H. Q. Wong, Y.-G. Gao, W. Hong, E. C. Y. Woon, *Sci. Rep.* **2016**, *6*, 25677.
[56] T. Yang, A. Cheong, X. Mai, S. Zou, E. C. Y. Woon, *Chem. Commun.* **2016**, *52*, 6181 – 6184.
[57] N. R. Rose, E. C. Y. Woon, A. Tumber, L. J. Walport, R. Chowdhury, X. S. Li, O. N. F. King, C. Lejeune, S. Ng, T. Krojer, M. C. Chan, A. M. Rydzik, R. J. Hopkinson, K. H. Che, M. Daniel, C. Strain-Damerell, C. Gileadi, G. Kochan, I. K. Leung, J. Dunford, K. K. Yeoh, P. J. Ratcliffe, N. Burgess-Brown, F. von Delft, S. Muller, B. Marsden, P. E. Brennan, M. A. McDonough, U. Oppermann, R. J. Klose, C. J. Schofield, A. Kawamura, *J. Med. Chem.* **2012**, *55*, 6639 – 6643.
[58] G. R. L. Cousins, S.-A. Poulsen, J. K. M. Sanders, *Chem. Commun.* **1999**, 1575 – 1576.
[59] R. Nguyen, I. Huc, *Chem. Commun.* **2003**, 942.
[60] B. Levrand, Y. Ruff, J.-M. Lehn, A. Herrmann, *Chem. Commun.* **2006**, 2965 – 2967.
[61] E. H. Cordes, W. P. Jencks, *J. Am. Chem. Soc.* **1962**, *84*, 826 – 831.
[62] I. K. H. Leung, E. Flashman, K. K. Yeoh, C. J. Schofield, T. D. W. Claridge, *J. Med. Chem.* **2010**, *53*, 867 – 875.
[63] M. Sindelar, T. A. Lutz, M. Petrera, K. T. Wanner, *J. Med. Chem.* **2013**, *56*, 1323 – 1340.
[64] E. C. Y. Woon, A. Tumber, A. Kawamura, L. Hillringhaus, W. Ge, N. R. Rose, J. H. Y. Ma, M. C. Chan, L. J. Walport, K. H. Che, S. S. Ng, B. D. Marsden, U. Opperman, M. A. McDonough, C. J. Schofield, *Angew. Chem. Int. Ed.* **2012**, *51*, 1631 – 1634; *Angew. Chem.* **2012**, *124*, 1663 – 1666.
[65] I. K. H. Leung, M. Demetriades, A. P. Hardy, C. Lejeune, T. J. Smart, A. Szöllössi, A. Kawamura, C. J. Schofield, T. D. W. Claridge, *J. Med. Chem.* **2013**, *56*, 547 – 555.

Manuscript received: May 9, 2018
Revised manuscript received: June 12, 2018
Accepted manuscript online: June 19, 2018
Version of record online: September 14, 2018